Applied Catalysis B: Environmental 189 (2016) 151–159

Contents lists available at ScienceDirect

Applied Catalysis B: Environmental

journal homepage: www.elsevier.com/locate/apcatb

Influence of atmospheric plasma spraying on the solar photoelectro-catalytic properties of TiO_2 coatings

Sergi Dosta[a,*], Marco Robotti[a], Sergi Garcia-Segura[b,**], Enric Brillas[b], Irene Garcia Cano[a], Josep Maria Guilemany[a]

[a] CPT Thermal Spray Center, Materials Engineering, Departament d'Enginyeria Química I Metal·lúrgica, Universitat de Barcelona, Martí i Franquès 1, E-08028 Barcelona, Spain
[b] Laboratori d'Electroquímica dels Materials i del Medi Ambient, Departament de Química Física, Facultat de Química, Universitat de Barcelona, Martí i Franquès 1, E-08028 Barcelona, Spain

ARTICLE INFO

Article history:
Received 7 November 2015
Received in revised form 19 February 2016
Accepted 22 February 2016
Available online 26 February 2016

Keywords:
Acid orange 7
Athmospheric plasma spray
Solar photoelectrocatalysis
Titanium dioxide coatings
Water treatment

ABSTRACT

Titanium dioxide is a widely available material which possesses outstanding properties, chemical stability and low cost. This paper reports the synthesis of nine TiO_2 coating from three commercial TiO_2 rutile and anatase and TiO_{2-x} sub-oxide powders onto Inconel alloy substrates by means of atmospheric plasma spray (APS). The influence of this thermally-activating technique on TiO_2 powder feedstocks, the role of its spraying conditions as well as the importance of the final active behavior of the coatings were studied. The performance of the coatings as photoanodes in the solar photoelectrocatalysis (SPEC) treatment of a model azo dye was explored. APS spraying parameters were selected in order to achieve a well-bonded coating, a determined thickness and a specific surface roughness. Moreover, Argon feeding gas of plasma torch played an important role in the quick melting process, particularly related to the heat transferred to the TiO_2 particles and the achievement of non-stoichiometric TiO_2. The prepared coatings were coupled to an air-diffusion cathode inside a photoelectrochemical cell and directly exposed to sunlight irradiation. Through XRD, SEM and surface characterization of the different coatings, the properties of the best TiO_2 material for the dye degradation by SPEC were elucidated.

1. Introduction

Titanium dioxide (TiO_2) is one of the materials of the next future due to their mechanic characteristics, biocompatibility and high stability and photocatalytic properties [1]. Taking advantage of such photocatalytic properties, TiO_2 can be employed in a wide spectrum of different advanced functional material applications such as auto-cleanable surfaces or decontamination devices to improve environmental quality [1–3]. The photocatalytic properties of TiO_2 are related to its semiconductor condition. When TiO_2 is irradiated with UV light, the transition of an electron from the filled valence band to the empty conduction band is promoted by Reaction (1), with an energy band gap of 3.2 eV, generating highly oxidative holes (h_{vb}^+) and reductive electrons (e_{cb}^-) [1,4]. The holes thus formed can react with water either from air humidity or from an aqueous media generating hydroxyl radical ($^\bullet OH$) from Reaction (2), the second most oxidizing species known after fluorine [3–5].

$$TiO_2 + h\nu \rightarrow e_{cb}^- + h_{vb}^+ \quad (1)$$

$$h_{vb}^+ + H_2O \rightarrow {}^\bullet OH + H^+ \quad (2)$$

However, the photocatalytic activity is strongly lost due to the fast recombination of electrons promoted to the valence band either with unreacted holes by Reaction (3), returning to the ground state [4,5].

$$e_{cb}^- + h_{vb}^+ \rightarrow TiO_2 + \text{heat} \quad (3)$$

It is known that the specific area of TiO_2 irradiated plays an important role on its photocatalytic efficiency. A higher area allows a major promotion of Reaction (1) to compensate the efficiency lost by Reaction (3) and hence, TiO_2 nanoparticles present better photocatalytic performances than bigger shapes [1,6]. Despite this advantage, the problematic manipulation of TiO_2 nanoparticles along with their possible health hazardous effects [7,8], and the difficult recovery after usage [9,10] have avoided the application of these functional photocatalytic materials [2]. Supporting

* Corresponding author.
** Corresponding author.
E-mail addresses: sdosta@cptub.eu (S. Dosta), sergigarcia@ub.edu, sergigs_87@hotmail.com (S. Garcia-Segura).

http://dx.doi.org/10.1016/j.apcatb.2016.02.048
0926-3373/

the nanoparticles onto substrates has been proposed as a possible solution to the aforementioned handicap [11–13]. However, the considerable diminution of exposed area to UV illumination owing to the formation of nanoparticles conglomerates mined the photocatalytic efficiency of the resulting coating [14,15].

During the last years, photoelectrocatalysis (PEC) has been considered a valuable advanced oxidation process (AOP) to solve the nanoparticles handicaps and the loss in photocatalytic efficiency of easily operable surfaces of TiO_2 such as thin-films [16–21], nanotubes [22–26], or coral structures [27,28]. The application of either a constant bias anodic potential [17,22] or a low constant anodic current density (j_{anod}) [19,29] to the TiO_2 subjected to UV illumination in PEC allows extracting the photoinduced electrons by an external electrical circuit, thus inhibiting the recombination Reaction (3) and consequently, improving the photocatalytic performance [16,29,30]. Nevertheless, to homogenize the electric distribution onto the TiO_2 surface, it is highly recommended the use of a conductive substrate like a metal in contact with TiO_2. The preparation of stable TiO_2 coatings by affordable technologies is the last challenge to overcome [17,19,21,29]. In this context, atmospheric plasma spray (APS) is a technique that produces highly stable coatings, particle by particle from molten, semi-molten or solid particles onto a substrate. Previous studies have shown that it possesses ability enough to coat large areas in short manufacturing time with an excellent specific surface layer, which is expected to improve the photocatalytic performance of TiO_2 [31,32]. The control of the synthesis parameters in APS is fundamental since they directly affect the surface characteristics and the phase composition of the coatings, thus allowing modulating the intrinsic properties of prepared TiO_2 [33].

The main aim of the present work is to prove the applicability of APS to obtain highly stable TiO_2 coatings with a wide range of structural characteristics for their application as photoanodes. The influence of the synthesis parameters on the photoelectrocatalytic performances of the different TiO_2 coatings was evaluated by means of the decolorization efficiency of a solution of a model azo dye like Acid Orange 7 (AO7) using natural solar light as inexpensive and renewable UV source in the so-called solar photoelectrocatalysis (SPEC) process.

2. Experimental

2.1. APS technology and TiO_2 coating

Thermal spray processes represent advanced techniques for coatings manufacturing. Inside this wide field, APS is known as particle-by-particle depositing method of molten, semi-molten or solid micrometric materials onto a substrate. The powder feedstock material to be sprayed is accelerated by means of a high energetic stream. The high temperatures (5000–20000 °C) and particles velocities (100–600 m s^{-1}) of the plasma jet permit to melt materials with a high melting point. During the permanence time of the particles in the hot zone of plasma jet, mixing and homogenization phenomena occur and facilitate the following deposition and coating build-up steps. The quality of coatings strongly depends on spraying parameters such as powder particle size distribution, velocities, stand-off distance, gas stream temperature, transferred heat, coefficient of thermal expansion, heat and mass flows. Particles deformation in-flight behavior of the sprayed particles is fundamental to achieve good bonding, desired thickness and final top surface roughness of the products.

To prepare the TiO_2 coatings, an APS A-3000 system with an F4 plasma torch was used, together with an ABB three-dimensional 3D robot. This facility permits to reach high deposition efficiencies, coat large areas of different substrates in low manufacturing time and produce specific surface active layers. Different Ar/H_2 gas mixtures were used and they influence the heat transferred to the particles during their permanence inside the plasma. The Ar/H_2 ratios were modified, together with the plasma intensity, in order to change the phase composition of the coatings.

Table 1
Spraying conditions values for different samples.

Sample	Intensity [A]	Ar/H_2 ratio	Distance [mm]
A1	400	2.9	140
A2	600	2.9	120
A3	600	3.4	100
B1	400	2.9	140
B2	600	2.9	120
B3	600	3.4	100
C1	400	2.9	140
C2	600	2.9	120
C3	600	3.4	100

2.2. Chemicals

TiO_2 rutile (Powder A) and anatase (Powder C) commercial powders were both supplied by Sulzer Metco, whereas TiO_{2-x} sub-oxide (Powder B) commercial powder was supplied by Starck Amperit. These nano-agglomerated powders were used as starting feedstocks to manufacture the final coatings using Inconel alloy as substrate. Table 1 summarizes the spraying conditions that were used to obtain the final TiO_2 coatings.

Pure azo dye AO7 was purchased from Acros Organics and used as received to test the photocatalytic activity of the synthesized TiO_2 coating by APS. Sodium sulfate used as background electrolyte to improve the conductivity of test solutions was of analytical grade supplied by Fluka. Synthetic dye solutions were prepared with high-purity water obtained from a Millipore Milli-Q system with resistivity >18 MΩ cm at 25 °C and their pH was adjusted to 7.0 with analytical grade sulfuric acid or analytical sodium hydroxide, both supplied by Merck.

2.3. SPEC tests

The photoelectrochemical reactor consisted in an undivided, open and cylindrical cell with a double jacket in which external water circulated to maintain the solution temperature at 35 °C using a Thermo Electron Corporation HAAKE DC 10 thermostat to avoid water evaporation under sunlight exposition as described in previous work [29]. These trials were carried out under vigorous stirring with a magnetic bar at 800 rpm to ensure homogenization and the transport of reactants toward/from the TiO_2 coating used as electrode. The different synthesized TiO_2 coatings were used separately as photoanodes with 5 cm^2 electroactive area exposed to sunlight and tilted 41° from the solution surface to better collect the direct sun rays in our laboratory of Barcelona (latitude: 41° 21′N, longitude: 2° 10′E). The cathode was a 3 cm^2 carbon-PTFE air-diffusion electrode supplied by E-TEK and mounted as described elsewhere [34]. This cathode was fed with air pumped at 300 mL min^{-1} to generate H_2O_2 from Reaction (4). At the anodic current density of j_{anod} = 1.0 mA cm^{-2}, 1.66 mM of H_2O_2 were detected in solution after 180 min of treatment, indifferently of the photoanode used. This concentration represents about a 60% of the 2.76 mM H_2O_2 expected for a 100% current efficiency, probably due to its oxidation to O_2 gas at the TiO_2 photoanode yielding the weaker oxidant $HO_2^{\bullet}$ as intermediate from Reactions (5) and (6) [5,14]. This cathode was chosen because it prevents any possible reduction of the azo dye and its by-products [5].

$$O_2 + 2H^+ + 2e^- \rightarrow H_2O_2 \quad (4)$$

$$H_2O_2 \rightarrow HO_2^{\bullet} + H^+ + e^- \quad (5)$$

$$HO_2^{\bullet} \rightarrow O_2 + H^+ + e^- \quad (6)$$

The electrochemical assays were performed with 100 mL of solutions containing 0.050 M Na_2SO_4 as background electrolyte at pH 7.0 and constant j_{anod} = 1.0 mA cm^{-2} provided with an Amel 2053 potentiostat-galvanostat, as optimum operational parameters determined in previous work [29]. The experiments were made in sunny and clear days during the summer of 2014, with similar average irradiance of 31.0 W m^{-2} between 300 and 400 nm, as measured with a Kipp & Zonen CUV 5 radiometer.

2.4. Apparatus and analytical procedures

The particle size distribution of the three different feedstocks A (100% TiO_2 rutile), B (TiO_{2-x}) and C (100% TiO_2 anatase) commercial powders were measured by laser scattering using a Beckman Coulter LS 13 320 equipment. TiO_2 coating samples were cut and mounted in a conductive phenolic resin (Konductomet, Buehler) followed by the metallographic preparation. Optical microscope (DMI 5000 M, Leica) images of the cross section have been carried out in order to measure the thickness of the coatings. Afterwards, cross-section areas of the coatings as well as their surface morphologies have been studied by scanning electron microscopy (SEM) (JSM-5310, JEOL). Phase composition and quantification of feedstock powders were analyzed with an X'Pert PRO MPD diffractometer (PANalytical). The phase analysis of the different coatings were performed by X-ray diffractometry (XRD) using a Siemens D500 system type Bragg-Brentano θ/2θ by applying a Cu Kα_1 radiation ($\lambda(\alpha_1)$ = 0.15406 nm) at 45 kV and 40 mA current. The ratio between the obtained crystalline phases was determined using the calculation support of X'pert HighScore Plus software. A Matrox Inspector software image analyzer was used to quantify the porosity percentage of the coatings. The photocatalytic surface of the TiO_2 coatings was measured with a Mitutoyo Surftest 301 equipment and its adhesion was measured with a Servosis MCH-102ME system through the ASTM C633 standard. Both 2D and 3D roughness parameters were analyzed using a confocal microscope LEICA DCM3D system with an objective of 10X magnification. Sensoscan image analysis was used for such data and surface roughness Sa and Sq parameters were obtained through a LeicaScan Mountain software.

Linear sweep voltammetry (LSV) was carried out with a conventional three-electrode one-compartment cell thermostated at 25 °C using an Ecochemie Autolab PGSTAT100 potentiostat-galvanostat controlled by an Autolab Nova 1.5 software. The working electrode was the A3 TiO_2 coating, the counter electrode was a Pt wire and the reference electrode was a Ag/AgCl/KCl(sat.) electrode (E° = 0.197 V/SHE). The linear sweep voltammograms were recorded for a 0.050 M Na_2SO_4 solution of pH 7.0 at anodic potential (E_{anod}) from 0 to 2.4 V and a scan rate of 1 mV s^{-1} under an Ar atmosphere after previous bubbling of this gas through the solution for 30 min. The analysis was conducted in the dark and under natural sunlight irradiation.

The pH of dyes solutions was controlled and adjusted using a Crison GLP 22 pH-meter. The photoelectrocatalyic performance of the TiO_2 coatings was monitored from the decay of the absorbance of the AO7 solution at the maximum wavelength (λ_{max}) = 484 nm, measured on the spectra recorded with a Shimadzu 1800 UV–vis spectrophotometer at 35 °C. The percentage of color removal or decolorization efficiency was calculated from the absorbance at initial time (A_0) and at time t (A_t) at the λ_{max} = 484 nm from the expression [5,34]:

$$\%\ Color\ removal = \frac{A_0 - A_t}{A_0} \times 100 \quad (7)$$

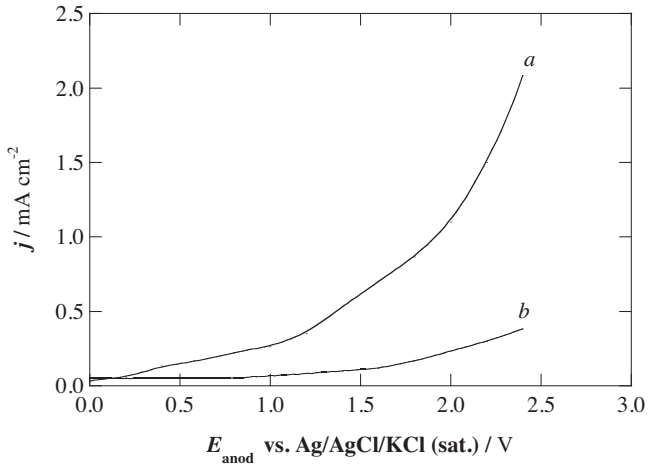

Fig. 1. Linear sweep voltammograms recorded for the TiO_2 coating A3 immersed in a 0.050 M Na_2SO_4 solution at pH 7.0 and 25 °C (a) under sunlight illumination and (b) in the dark. Initial anodic potential: 0 V, final anodic potential: 2.40 V. Scan rate 1 mV s^{-1}.

The AO7 concentration was followed during the photoelectrocatalytic treatments by reversed-phase high-performance liquid chromatography (HPLC) using a Waters 600 LC fitted with a Spherisorb ODS2 5 μm, 150 mm × 4.6 mm, column at 35 °C coupled to a Waters 996 photodiode array detector set a 484 nm. The chromatograms displayed a well-defined peak with retention time of 7.6 min after injection of 20 μL of sample into the LC using a mobile phase of 30:70 (v/v) acetonitrile/water mixture with 2.4 mM *n*-butylamine at 0.6 mL min^{-1}.

3. Results and discussion

3.1. Influence of crystalline and non-stoichiometric phases on SPEC performance

An initial blank experiment without any TiO_2 coatings did not undergo any loss of color of 100 mL of a 0.43 mM AO7 solution in 0.050 M Na_2SO_4 at pH 7.0 and 35 °C when 2 mM H_2O_2 was added to it either in the dark and under solar irradiation, indicating that the azo dye does not react with H_2O_2 electrogenerated at the cathode under SPEC conditions. Our previous work [29] evidenced a poor color loss by electrochemical oxidation in the dark and by direct photocatalysis under natural sunlight irradiation, where less than 45% and 20% decolorization were attained after 300 min of treatment, respectively. The present study was then focused on the photoelectrocatalytic response of the new TiO_2 coatings prepared by APS.

Taking into account that the use of galvanostatic experiments in photoelectrochemistry is problematic, since it does not allow to distinguish between photocurrents produced by light generating charge carriers and dark currents, comparative current density-E_{anod} curves for the A3 semiconductor anode in the background electrolyte at pH 7.0 were recorded in the dark and under natural sunlight illumination by means of LSV. As can be seen in Fig. 1, the photocurrent upon irradiation of the TiO_2 anode by sunlight (curve *a*) increased up to 6-fold compared to the current in the dark (curve *b*), thereby demonstrating the photoelectrocatalytic nature of the process under solar illumination.

To assess the photoelectrocatalytic efficiency of the prepared TiO_2 coatings, the above AO7 solution was degraded at j_{anod} = 1.0 mA cm^{-2} and the azo dye abatement was followed by HPLC for 180 min, time in which an almost complete removal of this compound (94%) was attained for the best coating performance,

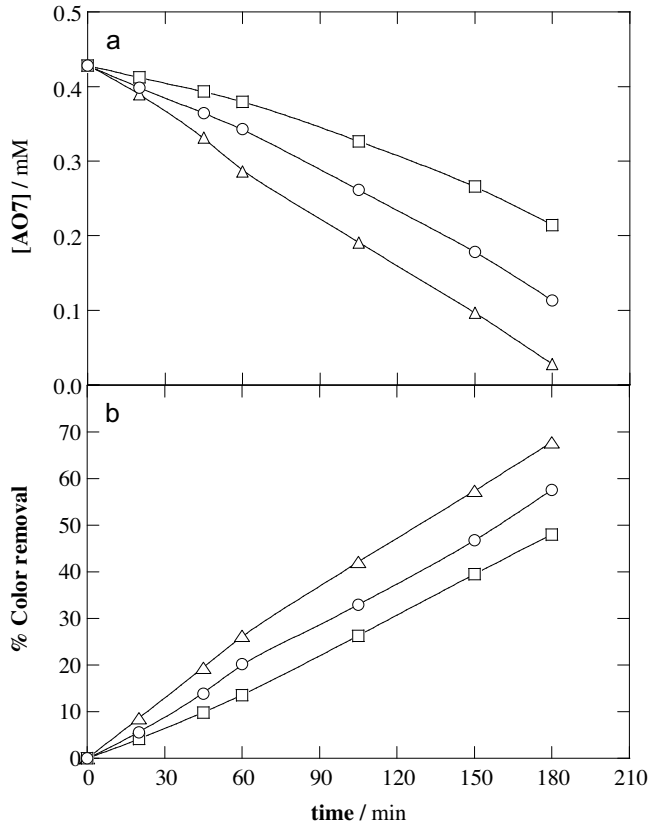

Fig. 2. (a) Acid Orange 7 (AO7) abatement followed by HPLC and (b) percentage of color removal measured by UV–vis at λ_{max} = 484 nm vs. time of the photoelectrocatalytic treatment of a 0.43 mM azo dye solution with 0.050 M Na_2SO_4 at pH 7.0 and 35 °C under natural sunlight irradiation by applying j_{anod} = 1.0 mA cm^{-2} for the TiO_2 coatings: (△) A3, (□) B3 and (○) C3.

Table 2
Crystalline and non-stoichiometric phases inside the prepared TiO_2 coatings.

Sample	Anatase [%]	Rutile [%]	Ti_3O_5 [%]	Ti_7O_{13} [%]	Ti_9O_{17} [%]
A1	2.0	13.0	38.0	18.0	29.0
A2	3.0	18.2	16.2	25.3	37.4
A3	4.0	20.0	18.0	23.0	35.0
B1	2.0	11.0	12.0	29.0	46.0
B2	3.0	10.0	10.0	28.0	49.0
B3	4.0	11.0	12.0	30.0	43.0
C1	3.0	13.0	12.0	26.0	46.0
C2	2.0	12.1	26.3	24.2	35.4
C3	4.0	12.9	11.9	28.6	42.6

as shown Fig. 2a. In all these trials, the solution pH was continuously regulated to its initial value of 7.0 by adding small volumes of 0.5 M NaOH. Fig. 2b highlights that the changes of the percentage of color removal at λ_{max} = 484 nm in such SPEC treatments showed significant differences of the photoelectrocatalytic activity depending on the synthesized coatings, leading to different decolorization kinetics. For this reason, the phase distribution of the TiO_2 coatings was analyzed by XRD as one of the feasible parameters that could explain their photoelectrocatalytic efficiency.

As stated above, the spraying conditions and the feedstock powder used could affect the final distribution of titanium oxide phases in the coating [31–33]. Consequently, it is possible to control the phase distribution in the coatings from the selection of spraying parameters. The XRD spectra of Fig. 3 evidence that the same final phases were found in all the coatings, indistinctly of the starting powder material (TiO_2 rutile, TiO_{2-x} sub-oxide or TiO_2 anatase) and conditions tested. However, different proportion of phases were formed depending on the experimental conditions, as can be seen in Table 2. The formation of new phases could be justified by the high temperatures of plasma that are able to promote the feedstock powder phase transformation [31–33]. Greater spraying temperature then made feasible to obtain a higher quantity of different sub-oxides or phases.

The results on the characterization of the synthesized titanium dioxide showed a predominance of non-stoichiometric phases (over 75%) in front of crystalline phases (anatase and rutile). The most influencing spraying parameter on the degree of crystallinity was the Ar/H_2 ratio of the plasma stream, since a greater Ar flow resulted in an increase of the percentage of crystalline phases. The melting and rapid solidification enhanced their presence and avoided the evolution to the rutile phase. Moreover, anatase appeared as a high-T metastable phase in a lower percentage in all coatings. When producing coatings through powders A (rutile) and C (mainly anatase), the same effect was observed. The proportion of sub-oxides increased rapidly when being sprayed, whereas there was some rutile (in the case of powder C) or anatase (in the case of powder A) coming from the rutile/anatase transformation during solidification. Finally, in the case of powder B (rutile and sub-oxides), the percentage of rutile was reduced due to an increase of the sub-oxide content during rapid solidification along with the transformation to anatase, because of the melting and resolidification process that led to similar percentages of this phase in all the coatings obtained through powders A and C.

The direct assessment of the phase distribution on the photoelectrocatalytical behavior of the coating on the color removal of the AO7 solution evidenced the noticeable higher photocatalytic character of the crystalline phases, as can be easily deduced from Fig. 4. It is important to remark that the crystalline phases of rutile and anatase present considerably lower band gaps (≤3.2 eV) than those of the non-stoichiometric phases (≥3.2 eV), thereby being

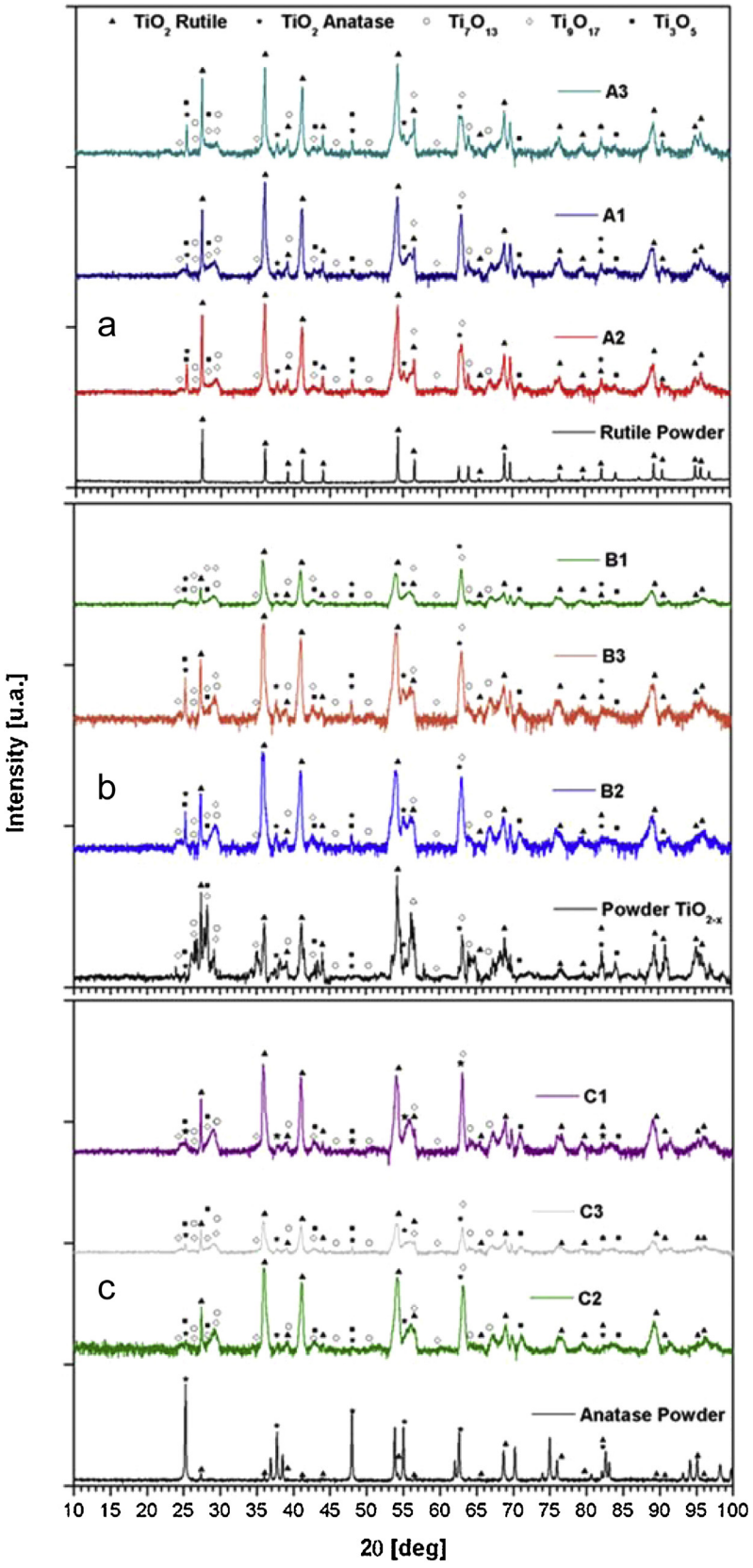

Fig. 3. X-ray diffractograms of the prepared TiO_2 photoanodes by atmospheric plasma spray (APS) technology using as precursor: (a) rutile powder, (b) TiO_{2-x} sub-oxide powder or (c) anatase powders, under the spraying conditions collected in Table 1.

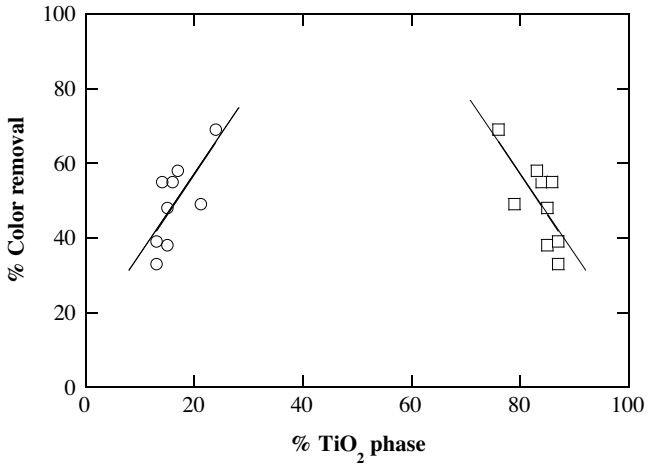

Fig. 4. Percentage of color removal at λ_{max} = 484 nm for 100 mL of a 0.43 mM Acid Orange 7 solution with 0.050 M of Na_2SO_4 at pH 7.0. and 35 °C under solar photoelectrocatalysis (SPEC) by applying j_{anod} = 1.0 mA cm^{-2} for 180 min in function of: (○) the percentage of crystalline phases of TiO_2 and (□) the percentage of amorphous phases of TiO_2.

easier the photo-promotion of the valence band electrons to the conductive band from Reaction (1) [1,23]. Nonetheless, titanium sub-oxides improve the electrical behavior of the coatings enhancing the recombination Reaction (3) between electrons and holes, although they are also able to increase the conductivity of the prepared materials, which is a functional property of interest for their application as photo-anodes.

3.2. Relationship between structural characteristics and photoelectrocatalytic response

The photoelectrocatalytic performance of the synthesized TiO_2 coatings is not expected to be exclusively related to their chemical composition but also to other important microstructural characteristics. The contribution and relevance of each measurable property on the photoelectrocatalytical response of prepared materials was then explored.

First of all, coatings micrographs were obtained by SEM. Fig. 5 highlights the cross section micrographs of the coatings synthesized using the three different feedstocks of A (TiO_2 rutile), B (TiO_{2-x}) and C (TiO_2 anatase). The most noticeable difference was associated to the thickness achievable under the same conditions for the different powders, being the thinner coatings those obtained with anatase powder. This effect is due to the stockpowder used. The powder morphology, apparent density and intern porosity affected the powder interaction with the flame torch of APS and influenced directly the efficiency of the coating formation and its thickness. Nevertheless, the coatings presented the same types of TiO_2 phases regardless of the feeding powder, as pointed out above.

It is also remarkable that lower energetic spraying conditions led to a lower melting of the particles and consequently, to higher roughness and porosity in the coatings. On the contrary, higher energetic spraying conditions melted better the particles.

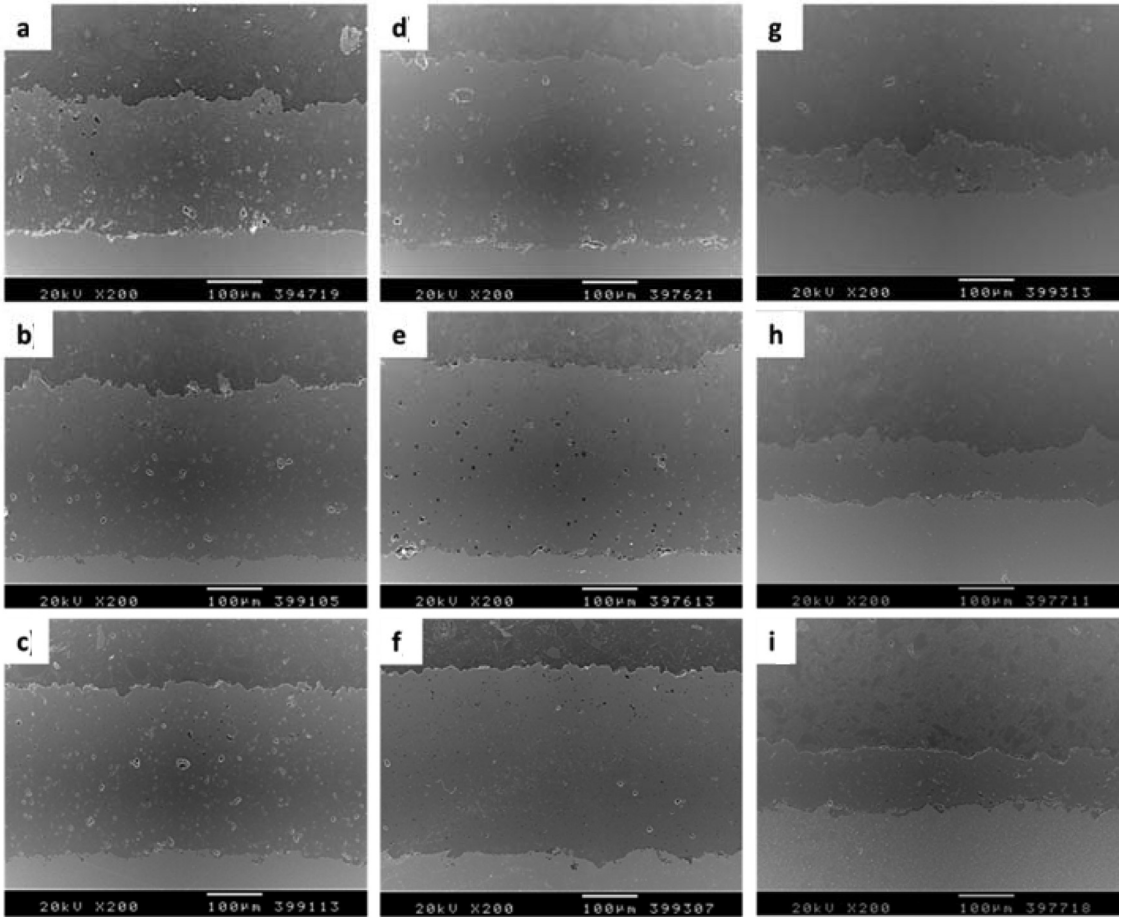

Fig. 5. Cross section scanning electron microscopy (SEM) micrographs of the TiO_2 coatings obtained by APS. Sample: (a) A1, (b) B1, (c) C1, (d) A2, (e) B2, (f) C2, (g) A3, (h) B3 and (i) C3.

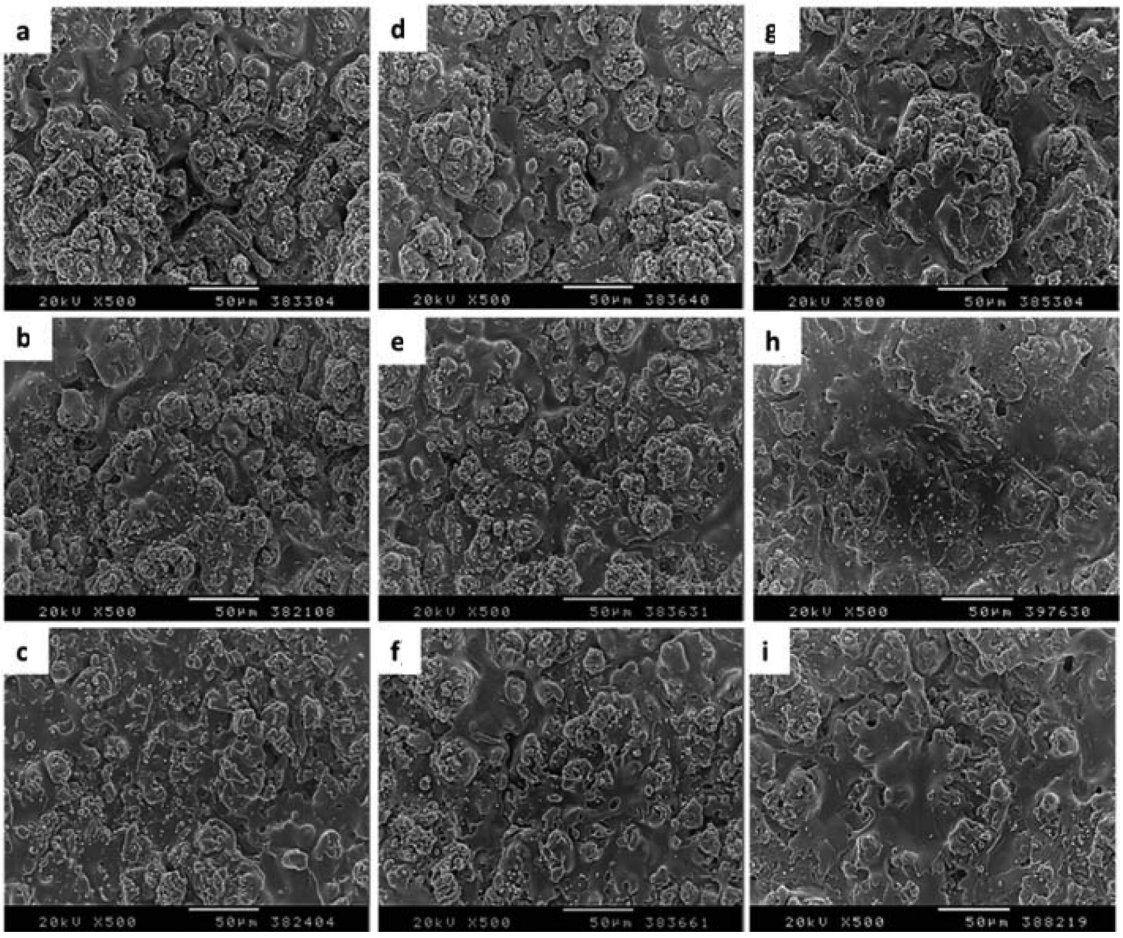

Fig. 6. SEM images of the free-surface of the TiO_2 coatings prepared by APS. Sample: (a) A1, (b) B1, (c) C1, (d) A2, (e) B2, (f) C2, (g) A3, (h) B3 and (i) C3.

Table 3
Experimental parameters determined for each prepared TiO_2 coating.

Sample	Thickness [μm]	Porosity [%]	Roughness Ra [μm]	Sa [μm]	Sq [μm]
A1	257.9 ± 9.9	9.5 ± 2.6	4.8 ± 0.1	4.9 ± 0.5	6.3 ± 0.7
A2	275.5 ± 9.5	11.4 ± 3.0	8.1 ± 0.4	6.1 ± 0.4	7.8 ± 0.5
A3	231.5 ± 15.5	9.9 ± 3.3	10.4 ± 0.4	7.7 ± 0.5	9.9 ± 0.7
B1	284.0 ± 6.9	10.1 ± 2.5	6.0 ± 0.2	4.7 ± 0.3	6.2 ± 0.3
B2	310.6 ± 17.7	6.9 ± 3.7	7.9 ± 0.9	5.4 ± 0.2	6.9 ± 0.2
B3	317.7 ± 24.7	5.6 ± 1.9	11.5 ± 3	6.1 ± 0.1	7.7 ± 0.1
C1	102.2 ± 14.8	11.3 ± 3.0	9.3 ± 0.5	7.4 ± 0.1	9.6 ± 0.1
C2	102.1 ± 15.4	9.6 ± 4.3	10.1 ± 0.6	7.0 ± 0.2	9.1 ± 0.3
C3	124.5 ± 14.1	14.4 ± 4.9	10.5 ± 0.3	7.1 ± 0.1	9.1 ± 0.1

The corresponding free-surface micrographs of the coatings depicted in Fig. 6 denoted significant differences between the coatings surfaces, also associated with the stockpowder used and the spraying conditions. Table 3 collects the characteristic parameters of each coating including thickness, porosity, 2D roughness and 3D surface values. These structural properties could have a marked influence on the intrinsic photocatalytic properties of the coatings that could be enhanced or diminished in function of their variation. To better clarify the extent of their possible influence, the decolorization efficiencies for 100 mL of the 0.43 mM AO7 solution at pH 7.0 after 180 min of SPEC treatment at j_{anod} = 1.0 mA cm^{-2} were represented against the measured values of each parameter, as shown in Fig. 7.

The coating thickness was not one of the most determining parameters on the photoelectrochemical behavior. Fig. 7a depicts that the percentage of color removal after 180 min of SPEC treatment rose slightly with increasing the film thickness up to 231.5 μm, whereupon dropped remaining around an average value of 45% for the thicker coatings. This kind of response is barely discussed in the literature as a result of two main effects. The first one is ascribed to the light penetration into the film to photogenerate the e_{cb}^-/h_{vb}^+ pair by Reaction (1). The maximum penetration depth of the incident light into the TiO_2 coating is defined by the function $1/\alpha$ according to Hitchman and Tian [21], where α is the absorption coefficient of TiO_2 at a defined wavelength allowing light penetation up to a maximum depletion layer width (W_{max}). Any species photogenerated within the W_{max} region could be efficiently diffused up to the coating surface when it is located in the minority carrier diffusion length of TiO_2. Thus, the increasing thickness of the TiO_2 coating could enhance the photogeneration of oxidants up to a limit, increasing the photoelectrocatalytic efficiency of the photoanode. The second effect related to the thickness is the coating conductivity. The SPEC process is based on the use of the TiO_2 as photoanode that implies the requirement of certain electric conductivity [16–29]. It is noticeable that the material resistivity (ρ) rises at higher thickness, diminishing the efficient removal of photo-promoted electrons by the external electric circuit [2,5]. This can explain the observed decay of the percentage of color removal for thicknesses >231.5 μm in Fig. 7a.

The porosity variation did not denote any considerable influence on the photoelectrocatalytic response, as can be deduced from Fig. 7b. Theoretically, an increase in porosity percentage should reduce the decolorization efficiency because lower photocatalyst would be present in the W_{max} region where the oxidant can be photogenerated [1,21], as stated above. Moreover, greater porosity could increase dramatically the material resistivity giving rise to

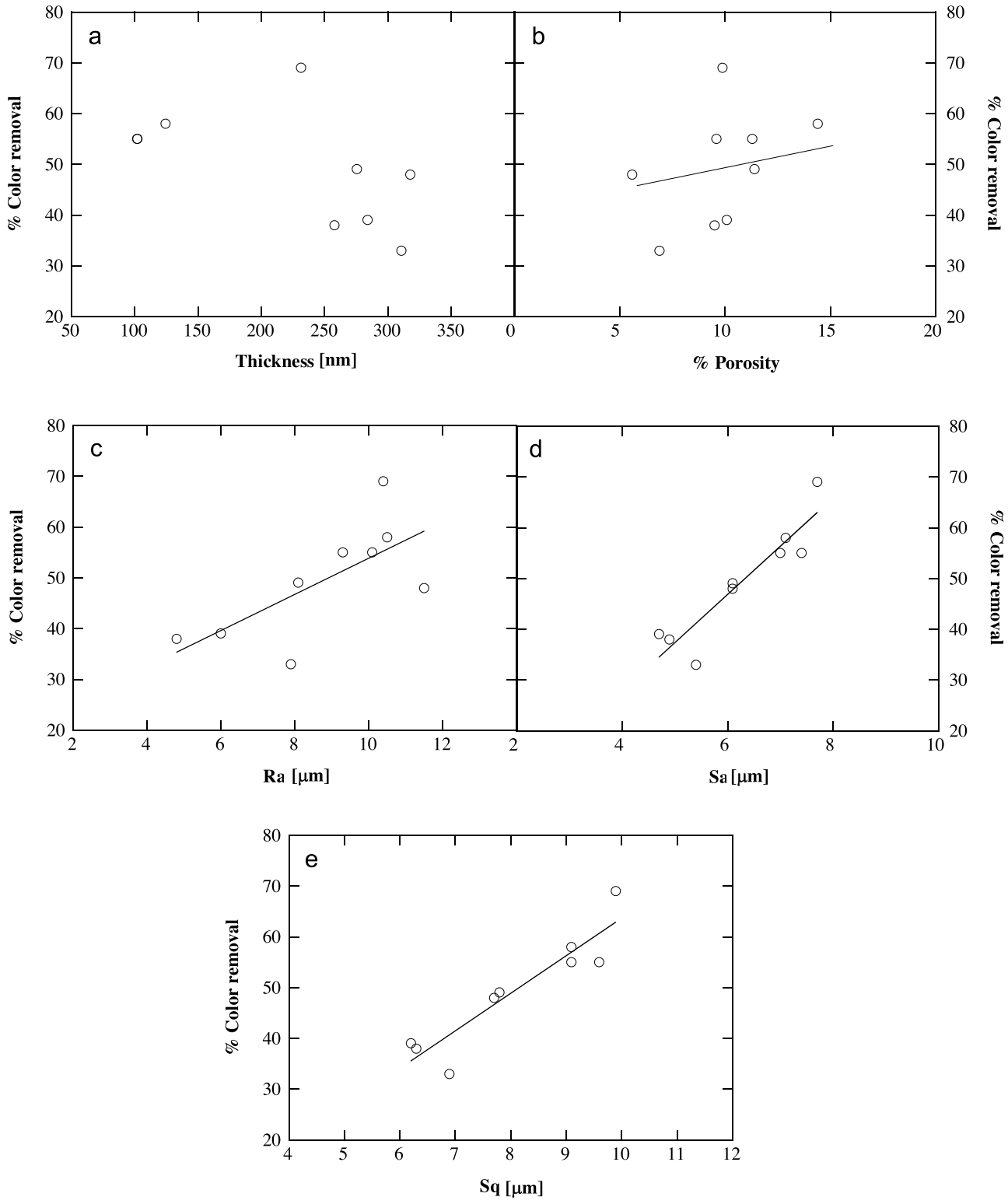

Fig. 7. Influence of the structural characteristics of the TiO_2 coating on the percentage of color removal at λ_{max} = 484 nm of 100 mL of a 0.43 mM Acid Orange 7 solution with 0.050 M of Na_2SO_4 at pH 7.0. and 35 °C by means of SPEC at j_{anod} = 1.0 mA cm^{-2} for 180 min. Coating parameters: (a) thickness, (b) porosity, (c) roughness, (d) superficial roughness average and (e) superficial roughness quadratic mean.

a lessening of the SPEC degradation [5]. However, these expected effects were not observed, probably due to the low porosity interval evaluated in the present work ranging from 5.6% to 14.4%.

The coating roughness was the main control parameter on the SPEC performance. Fig. 7c highlights that a higher decolorization was attained by the rougher surfaces. Nevertheless, this tendency was more apparent when considering the superficial roughness average (Sa) and the superficial roughness quadratic mean (Sq), shown in Fig. 7d and e, respectively. These two 3D roughness parameters give information about specific surfaces of the developed coatings which seem to be fundamental for SPEC applications. This technology is strongly related to surface processes [1–4], hence

higher photocatalytic generation of the e_{cb}^-/h_{vb}^+ pair by Reaction (1) is expected by greater specific area of TiO_2 irradiated. The SPEC decolorization of the treated AO7 solution then demonstrates that the available surface to be directly irradiated plays a remarkable role on the process efficiency. Moreover, the degradation process can be mediated by surface adsorption processes of the pollutants molecules to react with the adsorbed oxidants (mainly •OH and h_{vb}^+) that are more rapidly generated when a larger surface is exposed due to the higher number of catalytic sites [5,29].

Taking into account all the structural and phase distribution characteristics that are correlated with the SPEC efficiency for the decolorization of the AO7 solution, one can infer that the best synthesized coating acting as photoanode is the sample A3 since it contains the major proportion possible of crystalline phases (indistinctly rutile or anatase), the major roughness to dispose of a higher irradiation exposition area and an average thickness of about 230 μm to possess an appropriate electrical conductivity.

4. Conclusions

It has been shown that atmospheric plasma spraying is a promising technology to synthesize highly stable supported TiO_2 photocatalysts with good intrinsic properties for their use in SPEC processes for pollution remediation. The influence of the spraying conditions on the final structural and phase distribution of the coatings has been assessed, correlating these characteristics with their performance as photoanodes to decolorize an AO7 solution by SPEC. It has been found that the crystalline phases of TiO_2 (anatase and rutile) are more photocatalytic than non-stoichiometric TiO_2 sub-oxides. The coatings with higher proportion of crystalline phases then present better photoelectrocatalytic performances. However, the generated TiO_2 sub-oxides enhance the coatings conductivity favoring their application as photoanodes, being the presence of these phases also relevant for SPEC application. The structural characterization of the coatings revealed a slight influence of the TiO_2 thickness with an optimum value of about 200–230 μm. The property with higher influence resulted to be the 3D superficial roughness because the photocatalytic processes take place on the coating surface. When a larger specific area is available to be irradiated, a major photogeneration of oxidants occurs, with a considerable enhancement of the SPEC degradation of AO7. The best SPEC photoactivity was obtained for the coating A3 due to its major content of crystalline phases (rutile and anatase), greater 3D superficial roughness and appropriate thickness.

Acknowledgements

The authors wish to thank Generalitat de Catalunya (2014 SGR1558) and Ministerio de Economia y Competitividad (MINECO) from Spain, under the project MAT2013 46755R and the project CTQ2013-48897-C2-1-R co-financed with FEDER funds, for the financial support for this research work.

References

[1] A. Fujishima, X. Zhang, D.A. Tryk, Surf. Sci. Rep. 63 (2008) 515–582.
[2] K. Nakata, A. Fujishima, J. Photochem. Photobiol. C 13 (2012) 169–189.
[3] D. Friedmann, C. Mendive, D. Bahnemann, Appl. Catal. B: Environ. 99 (2010) 398–406.
[4] U.G. Akpan, B.H. Hameed, J. Hazard. Mater. 170 (2009) 520–529.
[5] E. Brillas, C.A. Martínez-Huitle, Appl. Catal. B: Environ. 166–167 (2015) 603–643.
[6] B. Bayarri, E. Carbonell, J. Gimenez, S. Esplugas, H. Garcia, Chemosphere 72 (2008) 67–74.
[7] B. Smolkova, N. El Yamani, A.R. Collins, A.C. Gutleb, M. Dubinska, Food Chem. Toxicol. 77 (2015) 64–73.
[8] R. Handy, M. Whitt, M. Rodriguez, M.J. Jackson, in: W. Ahmed, M. Jackson (Eds.), Emerging Nanotechnologies for Manufacturing, Elsevier, Oxford (UK), 2015, pp. 255–269.
[9] L. Dou, L. Gao, X. Yang, X. Song, J. Hazard. Mater. 203-204 (2012) 363–369.
[10] H. Choi, S.R. Al-Abed, D.D. Dionysiou, E. Stathatos, P. Lianos, in: I.C. Escobar, A.I. Schäfer (Eds.), Sustainable Science and Engineering, 2, Elsevier, Oxford (UK), 2010, pp. 229–254.
[11] S. Parra, S. Malato, C. Pulgarin, Appl. Catal. B: Environ. 36 (2002) 131–144.
[12] C. Guillard, J. Disdier, C. Monnet, J. Dussaud, S. Malato, J. Blanco, M.I. Maldonado, J.M. Herrmann, Appl. Catal. B: Environ. 46 (2003) 319–332.
[13] J. Marúgan, J. Aguado, W. Gernjak, S. Malato, Catal. Today 129 (2007) 59–68.
[14] B.R. Garza-Campos, J.L. Guzmán-Mar, L.H. Reyes, E. Brillas, A. Hernández-Ramírez, E.J. Ruiz-Ruiz, Chemosphere 97 (2014) 26–33.
[15] M. Jiménez-Tototzintle, I. Oller, A. Hernández-Ramírez, S. Malato, M.I. Maldonado, Chem. Eng. J. 273 (2015) 205–213.
[16] Y. Bennani, P. Appel, L.C. Rietveld, J. Photoch, Photobiol. A 305 (2015) 83–92.
[17] J. Marugán, P. Christensen, T. Egerton, H. Purnama, Appl. Catal. B: Environ. 89 (2009) 273–283.
[18] H. Zhang, Y. Wang, P. Liu, Y. Han, X. Yao, J. Zou, H. Cheng, H. Zhao, ACS Appl. Mater. Interfaces 3 (2011) 2472–2478.
[19] R. Daghrir, P. Drogui, M.A. El Khakani, Electrochim. Acta 87 (2013) 18–31.
[20] P.S. Shinde, P.S. Patil, P.N. Bhosale, A. Brüger, G. Nauer, M. Neumann-Spallart, C.H. Bhosale, Appl. Catal. B: Environ. 89 (2009) 288–294.
[21] M.L. Hitchman, F. Tian, J. Electroanal. Chem. 538 (2002) 165–172.
[22] Q. Zhang, J. Zhu, Y. Wang, J. Feng, W. Yan, H. Xu, Appl. Surf. Sci. 308 (2014) 161–169.
[23] J.C. Cardoso, T.M. Lizier, M.V.B. Zanoni, Appl. Catal. B: Environ. 99 (2010) 96–102.
[24] Z. Zhang, D. Pan, J. Feng, L. Guo, L. Peng, C. Xi, J. Li, Z. Li, M. Wu, Z. Ren, Mater. Lett. 66 (2012) 54–56.
[25] S.K. Mohapatra, M. Misra, V.K. Mahajan, K.S. Raja, J. Catal. 246 (2007) 362–369.
[26] X. Cheng, G. Pan, X. Yu, Chem. Eng. J. 279 (2015) 264–272.
[27] X. Hua, Y. Zhang, N. Ma, X. Li, H. Wang, J. Hazard. Mater. 172 (2009) 256–261.
[28] Y. Liu, K. Mu, G. Yang, H. Peng, F. Shen, L. Wang, S. Deng, X. Zhang, Y. Zhang, New J. Chem. 39 (2015) 3923–3928.
[29] S. Garcia-Segura, S. Dosta, J.M. Guilemany, E. Brillas, Appl. Catal. B: Environ. 132–133 (2013) 142–150.
[30] C. He, X.Z. Li, N. Graham, Y. Wang, Appl. Catal. A: Gen. 305 (2006) 54–63.
[31] M. Gardon, S. Dosta, J.M. Guilemany, M. Kourasi, B. Mellor, R. Wills, J. Power Sources 238 (2013) 430–434.
[32] M. Gardon, O. Monereo, S. Dosta, G. Vescio, A. Cirera, J.M. Guilemany, Surf. Coat. Technol. 235 (2013) 848–852.
[33] M. Gardon, C. Fernández-Rodríguez, M.R. Espino Estévez, S. Dosta, I.G. Cano, J.M. Guilemany, J. Therm. Spray Technol. 23 (2015) 1135–1141.
[34] X. Florenza, A.M.S. Solano, F. Centellas, C.A. Martínez-Huitle, E. Brillas, S. Garcia-Segura, Electrochim. Acta 142 (2014) 276–288.